Journal of Engineering and Technology for Industrial Applications

ITEGAM-JETIA

Manaus, v.12 n.58, p. 325-333. March/April, 2026.
DOI: https://doi.org/10.5935/jetia. v12i58.3063

ISSN ONLINE: 2447-0228

RESEARCH ARTICLE OPEN ACCESS

EXPERIMENTAL INVESTIGATION OF ROTARY FRICTION WELDING OF AL2017A ALLOY REINFORCED WITH ALUMINA (AL_2O_3) PARTICLES

Ahlem Mechta*[1], Elhadj Raouache[2] and Aissa Laouissi[3]

[1, 2, 3]Department of Mechanical Engineering, University of Mohamed El Bachir El Ibrahimi, Bordj Bou Arreridj, 34000, Algeria.

[1]https://orcid.org/0009-0002-0737-3574, [2]https://orcid.org/0009-0007-2063-0711, [3]https://orcid.org/0000-0002-5723-3863

Email: *ahlem.mechta_1@univ-bba.dz, elhadj.raouache@univ-bba.dz, aissou_011@yahoo.fr

ARTICLE INFO

Article History
Received: December 5, 2025
Reviewed: January 7, 2026
Accepted: January 14, 2026
Published: March 31, 2026

Keywords:
Rotary friction welding,
Similar joints,
Al2017 A aluminum alloys,
Alumina (Al2O3) particle.

ABSTRACT

A series of similar joints made from Al2017A aluminum alloy were produced through rotary friction welding, with localized reinforcement provided by alumina (Al_2O_3) particles, a ceramic known for its high hardness and extensive use in metal–matrix composites. These particles were placed at the weld interface by filling drilled holes of different diameters in the fixed component, allowing the influence of varying volume fractions on joint behavior to be examined. Tests of tensile strength and microhardness indicated that adding Al_2O_3 leads to a noticeable improvement in the mechanical performance of the welded joints when compared with those lacking ceramic reinforcement.

I. INTRODUCTION

Friction welding is a solid-state joining process whose principle has been known since the late 20th century [1]; however, its significant industrial development only began in 1956 in the former Soviet Union [2] before gradually spreading to the United Kingdom and the United States [3]. Classified as a forging process, friction welding relies on the generation of heat at the interface through the rapid rotation of one component under controlled axial pressure against another [4]. The heat generated, combined with plastic deformation, leads to a localized material flow that enables bonding in the solid state without ever reaching the melting temperature [5]. This unique feature eliminates the typical defects associated with fusion welding processes, such as solidification cracking, porosity, and pronounced metallurgical heterogeneities [6], [7].

This process offers several advantages, including the production of joints with high mechanical integrity, reduced cycle times, excellent repeatability, low energy consumption, and the possibility of complete automation, ensuring consistent quality [8], [9]. In addition, its environmentally friendly nature - no welding fumes, no UV or electromagnetic radiation, and no need for filler metals or shielding gases - makes it an attractive technology for demanding sectors such as aerospace, automotive, energy production, and mechanical engineering [10], [11]. Nevertheless, despite these advantages, the relationships between welding parameters (rotational speed, axial force, friction time), thermal cycles, microstructural evolution, and resulting mechanical properties remain insufficiently understood [12], [13]. This knowledge gap limits the optimization of process parameters and the development of reliable predictive models [14], [15], particularly when welding dissimilar materials or alloys that are sensitive to thermal gradients [16-20].

In this context, the present work proposes a detailed experimental investigation of rotary friction welding applied to 2017A aluminum alloy, reinforced with alumina (Al_2O_3) ceramic particles. The main objective of this study was to evaluate the effect of reinforcement content on the joint quality, microstructural characteristics, and mechanical performance. The selected materials, operating parameters, and characterization techniques are described in detail in this section. The experimental results were analyzed and discussed to highlight the material–process interaction mechanisms and provide recommendations for optimizing rotary friction welding. This study contributes to a better understanding of the influence of ceramic reinforcements on the behavior of aluminum weldments and paves the way for the design of higher-performance joints for advanced industrial applications.

II. MATERIALS AND METHODS

II.1 MATERIALS USED

II.1.1 Aluminum Alloy 2017A

Aluminum alloy 2017A, belonging to the 2XXX series (Al-Cu-Mg), is a structurally hardening alloy whose strength arises from the precipitation of $CuAl_2$ and $CuMgAl_2$ compounds. Its composition of copper (2.6-6.3%) and magnesium (0.5-1.5%) endows it with excellent mechanical properties. The addition of silicon and manganese (< 0.8%) improves the strength by dispersion, whereas iron degrades the hardening by forming undesirable compounds. Secondary alloying elements (such as Cr, Zn, and Ti) further optimize the performance of the aluminum alloys.

Table 1: Composition of alloy 2017A in mass percentage.

If	Fe	Cu	Mn	Mg	Cr	Zn	Zr + Ti	Each other	Total other	Al
0.20-0.80	≤ 0.70	3.5-4.5	0.4-1.0	0.4-1.0	≤ 1.0	≤ 0.25	< 0.25	≤ 0.05	≤ 0.25	Stay

Source: [21].

Table 2: Mechanical properties of aluminum 2017A.

∅(mm)	Rm (Mpa)	$\boldsymbol{Rp_{0.2}}$(Mpa)	HAS(% ***mini***)
$\emptyset \leq \mathbf{55}$	≥ 400	≥ 250	10

Source: [21].

II.1.2 Alumina AL_2O_3

Alumina (Al_2O_3) is a refractory oxide extracted from bauxite, very chemically stable and with a high melting point (≈ 2054 °C).

Table 3: Chemical composition of alumina (determined by XRF).

Compounds	Na2O	Cao	Mgo	Sio2	HAS $\boldsymbol{L_2O_3}$
Alumina	0.14	0.15	0.24	0.52	98.95

Source: Authors, (2026).

II.2 PREPARATION OF WELDED SAMPLES FOR MICROGRAPHIC OBSERVATION

This section investigates the preparation, microstructural analysis, and mechanical performance of aluminum joints produced by rotary friction welding. Metallographic preparation included sectioning, resin mounting, progressive SiC polishing, and etching with Keller's reagent. Optical microscopy (×10–×1000) was used to characterize weld-zone microstructure. Mechanical behavior was evaluated through Vickers microhardness (200 g, 10 s), tensile testing (W310), and three-point bending on a servo-controlled universal machine.

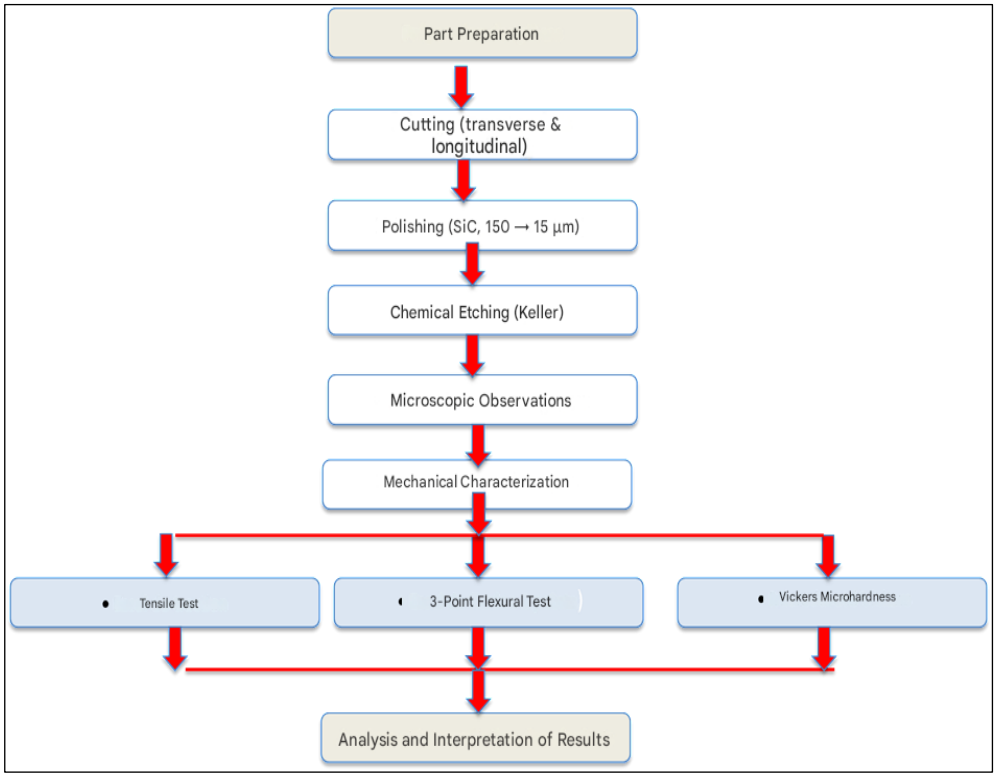

Figure 1: Experimental procedure for specimen preparation and characterization.
Source: Authors, (2026).

II.2.1 Cutting, Dressing and Drilling:

Before starting the rotary friction welding processes, the used 2017A rods were cut into samples with a length of 70 mm and a diameter of 12 mm. The ends of the samples were polished and cleaned.

II.2.2 Addition AL_2O_3

Volume fractions are calculated as follows:

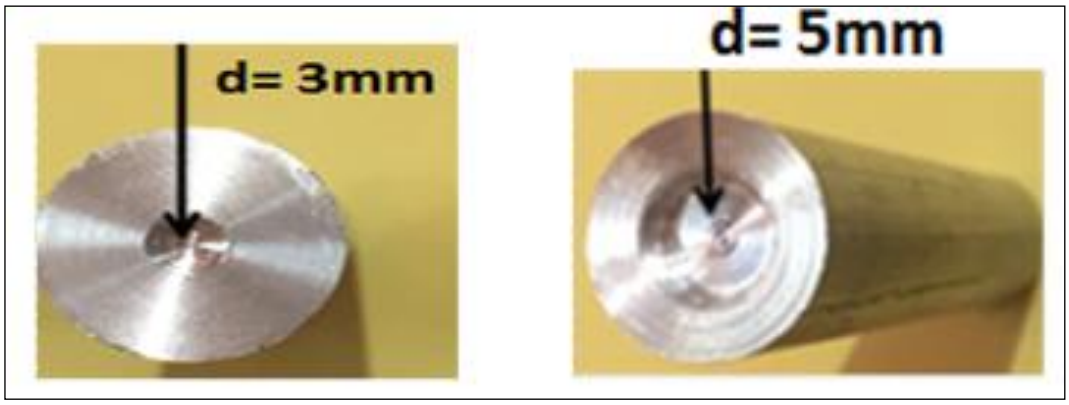

Figure 2: Experimental specimens illustrating the internal diameters investigated in the present study.

Diameters:

$$\begin{cases} d_0 = 0 \\ d_1 = 3mm \\ d_2 = 5mm \end{cases}$$

Area contact: $\frac{\pi d^2}{4}$

Volume fraction of aluminum:

$$100\% \quad \rightarrow \quad \frac{\pi d^2}{4}$$

$$X_i\% \quad \rightarrow \quad \frac{\pi d_i^2}{4}$$

Sample 1: $d_0 = 0 \Longrightarrow X_0 = 0\%$

Sample 2 : $d_1 = 3\ mm \Longrightarrow X_1 = 6.25\ \%$

Sample 3: $d_2 = 5\ mm \Longrightarrow X_2 = 17.36\%$

Before welding, Al_2O_3 particles were added at different volume fractions to the interface of the joints through pre-drilled holes, as shown in (Figure 3c). The experimental setup utilized a PMO UF 1.5 universal milling machine (Figure 3d) installed in the Mechanical Engineering Laboratory of the University of Bordj Bou Arreridj. The friction rotation welding process was performed on cylindrical specimens with a diameter of 12 mm and a length of 70 mm. The main welding parameters were as follows:

- Rotation speed: 1400 rpm
- Friction time (heating phase): 40
- Forging time (forging phase): 10 s
- Axial movement speed: 63 mm/min

To evaluate the maximum temperature attained during welding, temperature measurements were performed under various processing conditions. A thermocouple was used for temperature acquisition and was mounted on the rotating component, as shown in Figure 3e.

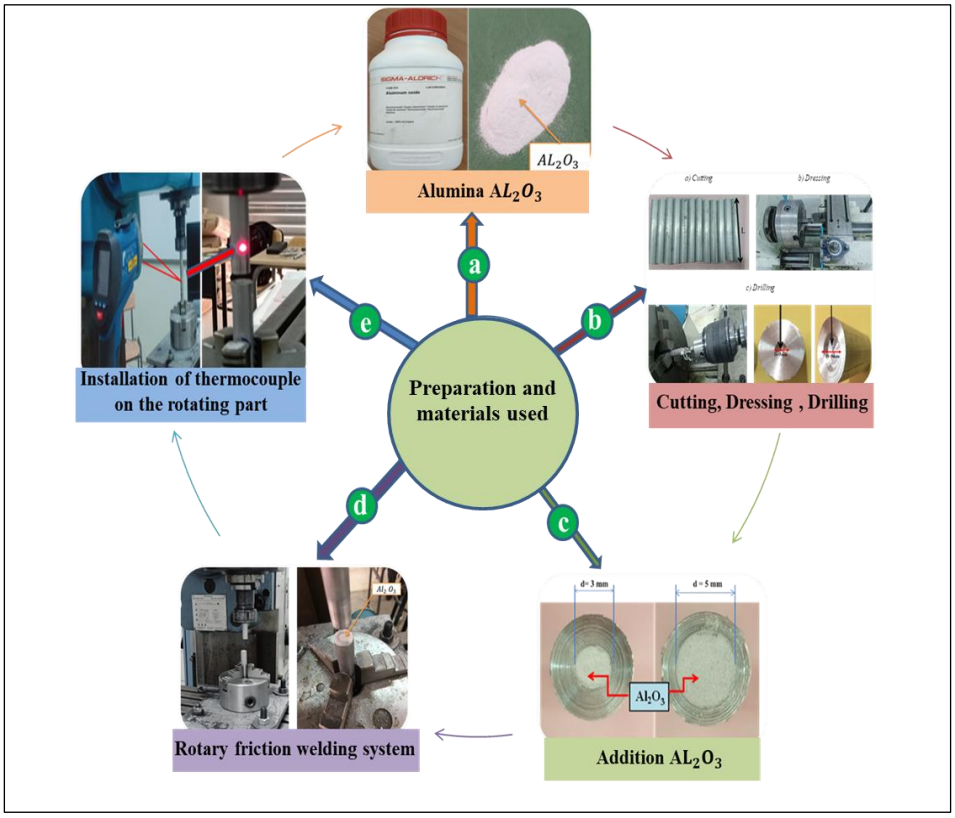

Figure 3: Materials and Experimental Procedures.
Source: Authors, (2026).

III.RESULTS AND DISCUSSIONS

III.1 VISUAL OBSERVATIONS:

After rotary friction welding, the bead of the aluminum/aluminum samples is asymmetrical and its size varies from one sample to another (Figure 4.1 and 4.2).

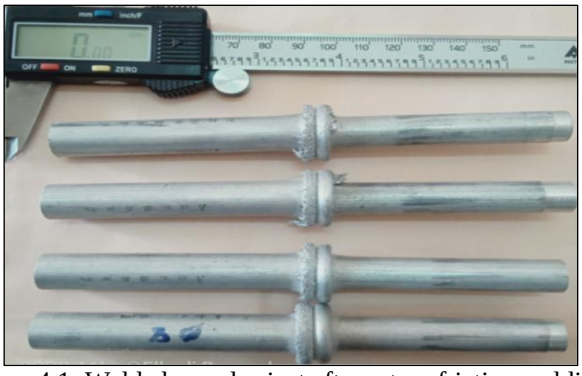

Figure 4.1: Welded samples just after rotary friction welding.
Source: Authors, (2026).

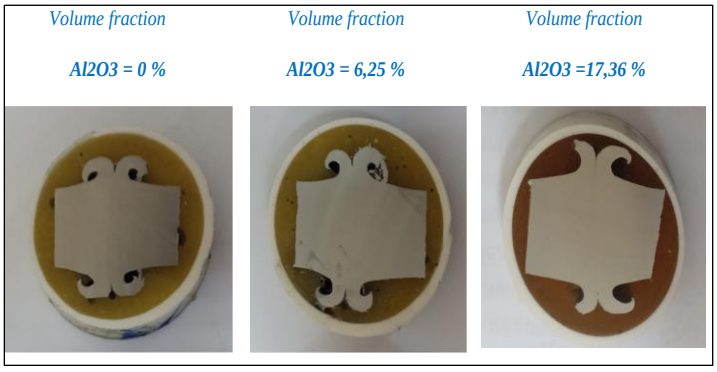

Figure 4.2: Longitudinal sections of welded samples.
Source: Authors, (2026).

III.2 SHORTENING OF WELDED JOINTS (BROWN-OFF)

Figure 5 illustrates the variation in burn-off as a function of the alumina (Al_2O_3) volume fraction in rotary friction-welded (RFW) joints. The results show that the burn-off does not vary linearly with the reinforcement content. As the Al_2O_3 fraction increases from 0% to 6.25%, the burn-off increases noticeably, reaching its maximum at approximately 6.25%. However, when the Al_2O_3 content is further increased to 17.36%, the burn-off decreases again, although it remains slightly higher than that of the unreinforced material. This trend reflects the combined effect of frictional heat generation and plastic flow resistance during welding. At moderate Al_2O_3 contents (≈ 6.25 %), the ceramic particles enhance interfacial friction and promote localized plastic deformation, resulting in increased material softening and expulsion from the interface.

This leads to the highest burn-off observed. Conversely, at higher reinforcement levels (17.36 %), the increased particle concentration acts as a rigid barrier that restricts plastic flow and reduces the effective heat generated at the interface. Consequently, less material is displaced, leading to a lower burn-off compared with the 6.25% sample. The lowest burn-off at 0% Al_2O_3 can be attributed to the absence of ceramic reinforcement, which limits frictional interaction and maintains a more uniform material flow. These observations are consistent with trends reported in the literature.

By [21] showed that the introduction of Al_2O_3 nanopowder during friction stir processing (FSP) can modify heat generation and improve mechanical behavior. According to [22] reported an optimal reinforcement level near 8 vol% for Al_2O_3-reinforced AA6082-T6 joints, where excessive ceramic content reduced heat input and plastic flow. Similarly [23] found that excessive nanoparticle additions impede material flow in the nugget zone, while [24] emphasized the role of particle concentration in governing thermal input and energy dissipation. Therefore, the maximum burn-off observed at a moderate reinforcement fraction (≈ 6.25 vol.% Al_2O_3) can be attributed to an optimal balance between enhanced frictional heating and sufficient material deformability, in agreement with previously reported behaviors in particle-reinforced friction-based processes.

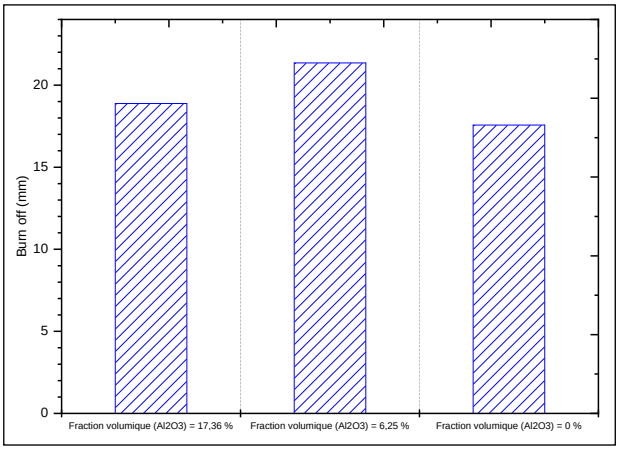

Figure 5: Burn off of welded joints.
Source: Authors, (2026).

III.3 THERMAL CYCLES

Figure 6 shows the evolution of temperature as a function of time for different volume fractions of Al_2O_3 (0%, 6.25%, and 17.36%). Although the three curves follow a similar thermal profile-characterized by a rapid rise, a maximum peak, and a subsequent cooling stage-the reinforcement volume fraction significantly affects both the amplitude and the kinetics of the thermal response. During the heating phase, increasing the Al_2O_3 content leads to a more pronounced rise in the peak temperature. The curve corresponding to 17.36% Al_2O_3 reaches the highest maximum temperature, consistent with the observations of [25], who demonstrated that the introduction of ceramic particles enhances the local stiffness of the composite and intensifies heat generation under mechanical loading due to increased internal friction and amplified deformation gradients. Furthermore, the relatively high thermal conductivity of Al_2O_3 promotes rapid redistribution of heat within the matrix, explaining the steeper ascent toward the thermal maximum. This behavior aligns with the conclusions summarized by [26], who emphasized the direct influence of ceramic phases on heat diffusion and accumulation in metal matrix composites.

During the cooling phase, the curve corresponding to 17.36% Al_2O_3 remains slightly higher than the others immediately after the peak, indicating a greater thermal inertia. A similar phenomenon was reported by [27], who showed that composites with high Al_2O_3 content exhibit cooling kinetics governed by the particle thermal conductivity and their low heat capacity. At longer times, all three curves converge toward a similar temperature range, reflecting the global thermal equilibrium of the system. This convergence is consistent with classical heat transfer models in heterogeneous composites, as described by [28], which predict the progressive homogenization of the thermal field regardless of the reinforcement fraction. Overall, the results confirm that the thermal response is strongly controlled by the Al_2O_3 volume fraction, a conclusion also reported by [29] for composites subjected to thermomechanical loading. High reinforcement levels promote significant thermal peaks-potentially beneficial for plastic flow but likely to increase the risk of thermal degradation-whereas lower fractions provide a more moderate thermal behavior and improved process stability.

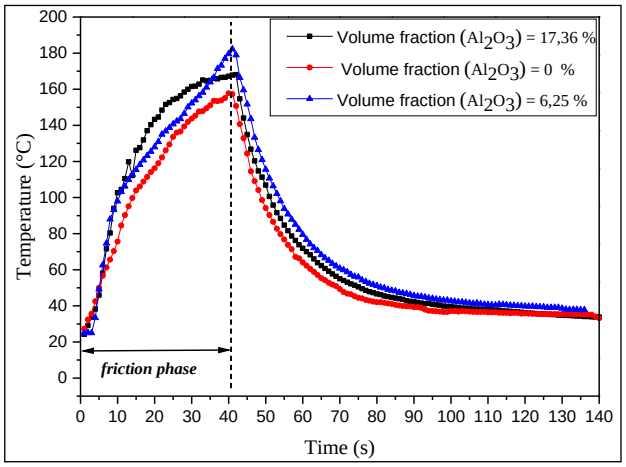

Figure 6: Temperature variations in the part (Aluminium 2017A, alumin AL_2O_3), during the welding process.
Source: Authors, (2026).

III.4 MICRO HARDNESS MEASUREMENTS

Vickers micro hardness was measured to determine the properties of the three zones of the welded joint: ZATM (plastically deformed), ZAT (heat-affected), and unaffected zones. For a sample with a volume fraction of 6.25%, a maximum hardness of 242.4 HV was observed near the weld interface without alumina. The rotating part generally has a higher hardness than the fixed part, whereas the central zone shows variable values (figure 7).

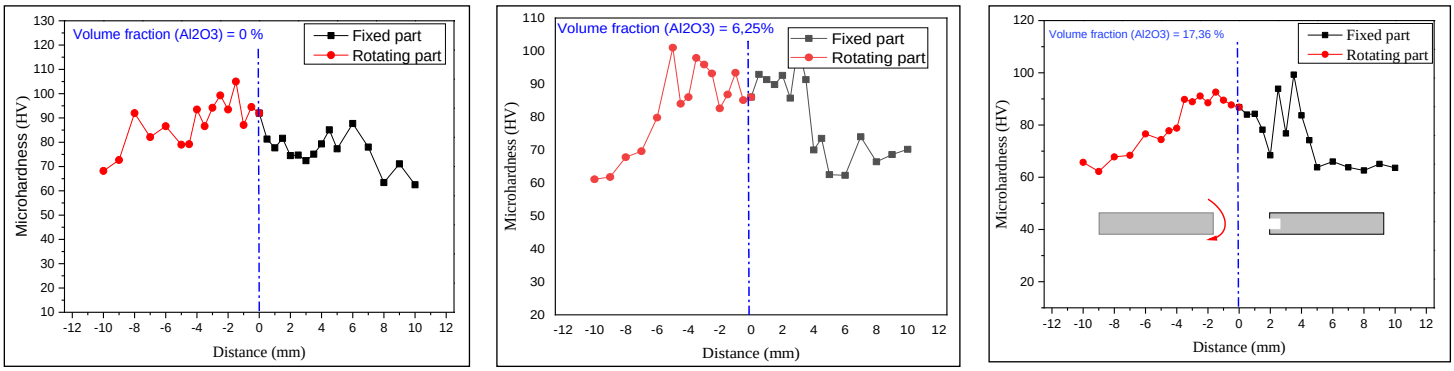

Figure 7: Microhardness profile.
Source: Authors, (2026).

III.5 TENSILE TEST

Tensile tests on the friction stir welded specimens showed that fracture occurred in the molten zone, indicating a homogeneous weld (Figure 8). The 6.25% volume fraction exhibited the best strength with a load of 16.62 kN, compared to 14.19 kN for the sample without alumina (0%).

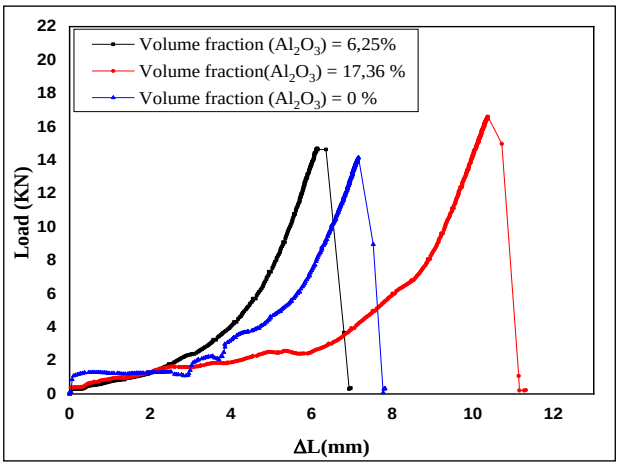

Figure 8: Traction curves for different volume fractions.
Source: Authors, (2026).

III.6 BENDING TEST

The welded joints were evaluated by three-point bending tests, carried out under identical conditions, with a distance between supports of 100 mm (Figure 9).

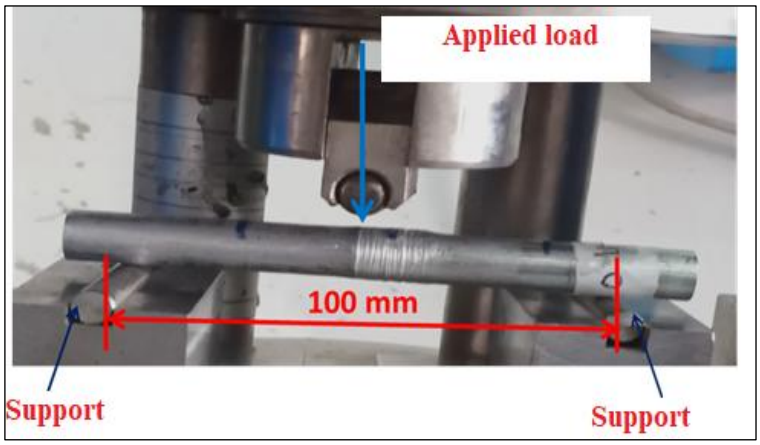

Figure 9: The principle of this test.
Source: Authors, (2026).

The simple and effective bending test was used to evaluate the strength of friction stir welded joints. The samples (Figure 10a) mainly deformed without fracture, with the maximum force versus time curves (Figure 10b) showing that only different bending angles were reached for samples 02 and 03.

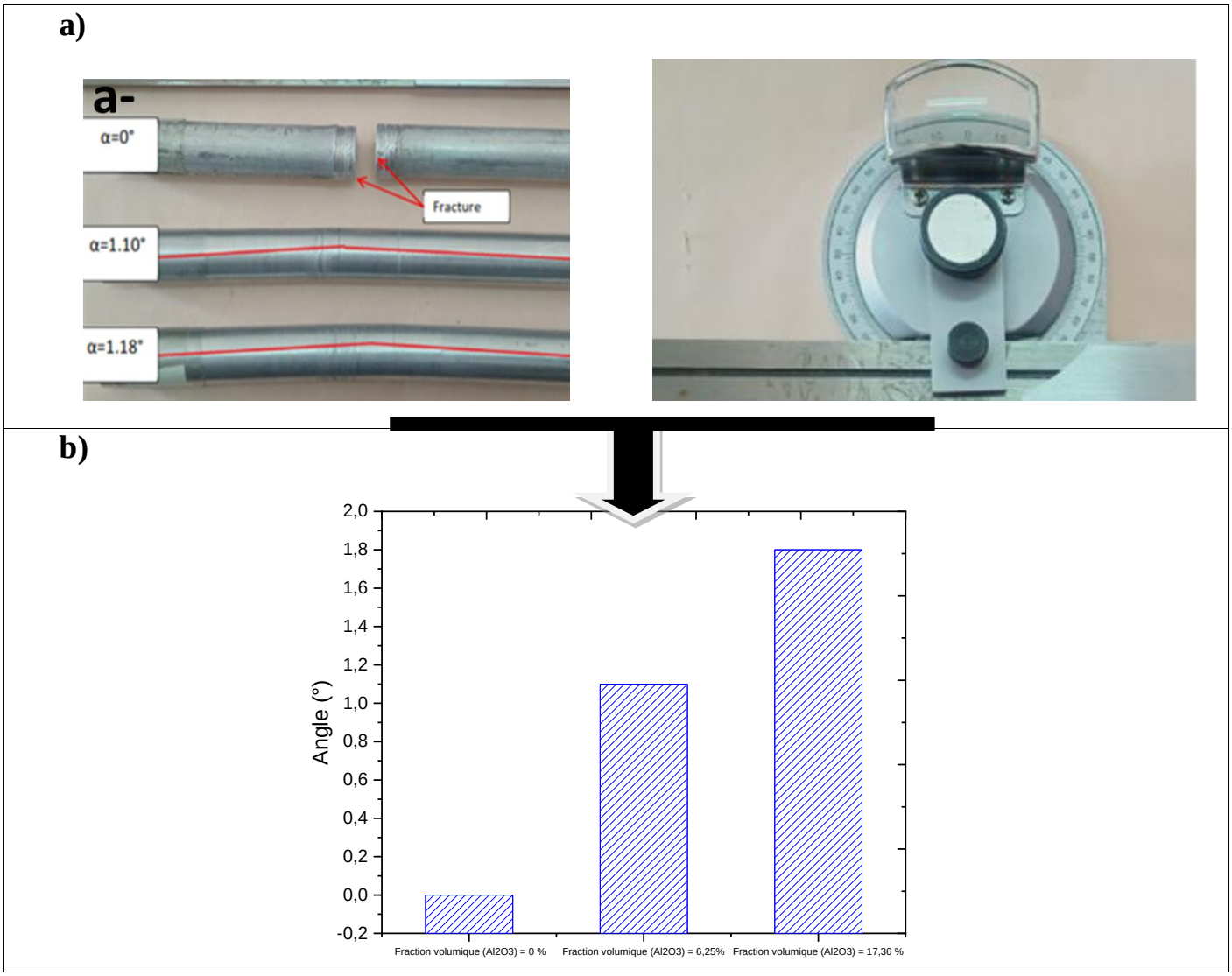

Figure 10.a: Specimens after bending test. Figure 10.b: Angle of different samples.
Source: Authors, (2026).

IV. CONCLUSIONS

This experimental study investigated the effect of alumina (Al_2O_3) particle addition on the rotary friction welding of 2017A aluminum joints. The weld bead formed on both parts, with its size varying between samples. The burn-off during welding and variations in welding parameters, such as the volume fractions, directly influence the heat generated and, consequently, the joint properties. Additionally, an increase in the traverse speed led to higher joint temperatures, reaching up to 450 °C. A maximum hardness of 242.4 HV was observed near the weld interface for a 6.25 % volume fraction in aluminum without Al_2O_3. Overall, the rotating part exhibited higher hardness than the fixed part, whereas the central zone of the weld exhibited variable values. The 6.25 % volume fraction also demonstrated superior mechanical performance, sustaining a maximum load of 16.62 kN. During the three-point bending tests, no rupture of the ductile materials occurred, and deformation occurred only at different angles.

V. AUTHOR'S CONTRIBUTION

Conceptualization: Ahlem Mechta and Aissa Laouissi.
Methodology: Ahlem Mechta and Elhadj Raouache.
Investigation: Ahlem Mechta and Aissa Laouissi.
Discussion of results: Ahlem Mechta, Elhadj Raouache and Aissa Laouissi.
Writing – Original Draft: Ahlem Mechta.
Writing – Review and Editing: Ahlem Mechta.
Resources: Ahlem Mechta.
Supervision: Ahlem Mechta and Elhadj Raouache.
Approval of the final text: Ahlem Mechta and Aissa Laouissi.

VI. REFERENCES

[1] W. M. Thomas and E. D. Nicholas, “Friction stir welding for the transportation industries,” Materials & Design, vol. 18, nos. 4–6, pp. 269–273, Dec. 1997.

[2] R. S. Mishra and Z. Y. Ma, “Friction stir welding and processing,” Materials Science and Engineering: R: Reports, vol. 50, nos. 1–2, pp. 1–78, Jan. 2005.

[3] P. L. Threadgill, A. J. Leonard, and R. G. Smith, “Friction-stir welding — recent developments,” Journal of Materials Processing Technology, vol. 133, nos. 1–2, pp. 5–14, 2003.

[4] T. Nandan, S. R. Mishra, and R. S. Mishra, “Modelling of friction stir welding,” Modelling and Simulation in Materials Science and Engineering, vol. 16, no. 3, 034006, 2008.

[5] M. J. Starink, A. Deschamps, and S.-C. Wang, “The strength of friction stir welded and friction stir processed aluminium alloys,” Scripta Materialia, vol. 58, no. 5, pp. 377–381, 2008.

[6] P. Colegrove and B. Shercliff (eds.), Friction Stir Welding and Processing VII — Proceedings, 2011.

[7] D. M. Neto and P. Neto, “Numerical modeling of the friction stir welding process — literature review,” arXiv preprint, Nov. 2013

[8] R. Rai, A. De, H. K. D. H. Bhadeshia, and T. DebRoy, “Review: friction welding tools,” Science and Technology of Welding and Joining, vol. 16, no. 4, pp. 325–342, 2011.

[9] TWI, “Technical knowledge on friction stir welding,” TWI Global, 2020.

[10] K. Mroczka, J. Dutkiewicz, and A. Pietras, “Microstructure of friction stir welded joints of 2017A aluminium alloy sheets,” Journal of Microscopy, vol. 237, no. 3, pp. 521–525, Mar. 2010.

[11] O. Mimouni, T. Nateche, N. Chekroun, M. Amara, M. H. Meliani et al., “Preparation, inspection, and optimization of rotary friction welding parameters for 2017A aluminum alloy specimens,” International Journal of Advanced Manufacturing Technology, vol. 134, nos. 9–10, pp. 4431–4450, Sep. 2024.

[12] A. Mani, A. Taherizadeh, B. Sadeghian, and P. Cavaliere, “Thermal–Mechanical and Microstructural Simulation of Rotary Friction Welding Processes by Using Finite Element Method,” Materials, vol. 17, no. 4, 815, 2024.

[13] N. Chakroune, T. Nateche, M. Amara et al., “Identification of the mechanical properties and surface morphology of friction welding on aluminum alloy specimens,” International Journal of Advanced Manufacturing Technology, vol. 130, pp. 2407–2421, 2024.

[14] M. Krbata, M. Kohutiar, S. Balos, and M. Pecanac, “The effect of rotary friction welding conditions on the microstructure and mechanical properties of Ti6Al4V titanium alloy welds,” Materials, vol. 16, no. 19, 6492, 2023.

[15] R. Kaibyshev, S. Suwas, S. V. Kailas et al., “Investigation on friction stir welding parameters: mechanical properties, correlations and corrosion behaviors of aluminum/titanium dissimilar welds,” Crystals, vol. 14, 305, 2024.

[16] “Static and fatigue behaviors of rotary friction welded AA7075 joints,” AIP Conference Proceedings, vol. 2860, 030006, 2024.

[17] M. A. Tashkandi, “Increasing of the Mechanical Properties of Friction Stir Welded Joints of 6061 Aluminum Alloy by Introducing Alumina Particles,” Advances in Materials Science, vol. 17, no. 2, 2017.

[18] S. K. Singh, R. K. Gautam, and A. K. Jha, “In-situ Al_2O_3 nanocomposites of metallic aluminum fabricated via friction stir processing,” Composites Part B: Engineering, vol. 198, 108221, 2020.

[19] M. F. Omar, N. A. A. M. Asri, and W. S. W. Harun, “A review on friction stir welding/processing: numerical modeling,” Metals, vol. 13, no. 8, 2023.

[20] L. Zhao, X. Wu, Y. Zhang, and Q. Liu, “Precipitation phenomena in Al_2O_3/Al-Mg-Si metal matrix composites manufactured via friction stir processing,” Journal of Alloys and Compounds, vol. 976, 172885, 2025.

[21] A. G. Mebarek, F. N. Mebrek, and A. H. Boukhoulda, “Effect of Al_2O_3 Nanopowder on the Mechanical and Microstructural Properties of AA5754 Alloy Processed by Friction Stir Processing,” J. Manuf. Mater. Process., vol. 8, no. 2, p. 58, 2024.

[22] A. Ouis, M. I. A. Habba, M. M. Z. Ahmed et al., “Tribological and corrosion behavior of Al_2O_3 interlayer reinforced friction stir welded AA6082-T6 joints,” Scientific Reports, vol. 15, Article no. 22437, 2025.

[23] P. K. Singh, V. N. Yadav, and R. K. Sharma, “Investigation on the Role of Al_2O_3 Nanoparticles in Enhancing Nugget Zone Properties during Friction Stir Welding,” Int. J. Mater. Process. Eng. Manuf., vol. 10, no. 3, pp. 45–54, 2025.

[24] S. Sharma and R. Patel, “Mechanical and Corrosion Studies of Nano-Al_2O_3 Reinforced Al-Mg Matrix Composites Fabricated by FSW Using RSM-ANN Modeling,” Symmetry, vol. 13, no. 4, p. 537, 2024.

[25] Z. Zhang, Y. Chen, L. Zhang, and H. Wu, “Influence of ceramic particle reinforcement on thermal–mechanical behavior of metal matrix composites,” Materials & Design, vol. 114, pp. 563–572, 2017.

[26] K. K. Chawla and N. Chawla, Metal Matrix Composites, 2nd ed. New York, NY: Springer, 2013.

[27] Yu, H., Zhang, Z., Li, Z., Huang, Y., & Liu, H., “Thermal conductivity and cooling behavior of Al_2O_3-reinforced polymer composites,” Composites Part B: Engineering, vol. 99, pp. 185–193, 2016.

[28] L. Hashin and S. Shtrikman, “A variational approach to the theory of the elastic behaviour of multiphase materials,” Journal of the Mechanics and Physics of Solids, vol. 10, no. 4, pp. 343–352, 1962.

[29] A. Adebisi, M. Maleque, and M. Rahman, “Metal matrix composite brake rotor: Thermal and stress analysis,” Journal of Materials Processing Technology, vol. 210, no. 9, pp. 1209–1217, 2014.